Growth and characterization of a nonlinear optical material L-serinium picrate monohydrate for optoelectronic applications

A. VICHITHRA[1], P. VASUDEVAN[1,*], E. VISWANATHAN[2], D. JAYARAMAN[3]
[1]*Department of Physics, Rajalakshmi Engineering College, Thandalam, Tamil Nadu, Chennai-602105, India*
[2]*Institute of Applied Nuclear Magnetic Resonance Research, Transzend Institute of Nuclear Magnetic Resonance, Transzend Scientific Pvt. Ltd, Electronic City, Bengaluru 560100, Karnataka, India*
[3]*Department of Physics, Presidency College, Chennai-600 005, Tamil Nadu, India*

L-serinium picrate monohydrate (LSPM) is an efficient nonlinear optical material with higher SHG efficiency, molecular flexibility, less lattice strain, thermal stability, high transparency and a reasonable optical band gap. Hence, the present work focuses on the growth and characterization of the LSPM single crystal. Single crystals of LSPM were successfully grown by slow evaporation technique. The grown crystal was subjected to XRD, FTIR, Optical absorption, Photoluminescence and thermal studies to understand the structural, lattice strain, optical and thermal properties of the material, and to correlate them with the NLO response. The grown crystal is found to possess a monoclinic system with non-centrosymmetric space group $P2_1$. Finally, the Kurtz-Perry powder technique was carried out to confirm the SHG efficiency of the material required for device fabrication.

(Received November 6, 2025; accepted April 8, 2026)

Keywords: Slow evaporation technique, XRD study, FTIR Analysis, Optical absorption study, SHG

1. Introduction

Researchers are very much interested in discovering new nonlinear single crystals because modern optoelectronic technologies such as lasers, optical communication, frequency conversion and photonic devices require materials with high efficiency, wide transparency, good stability, multifunctionality and environmental safety. Among various materials, amino acid-based materials have attracted considerable interest in nonlinear optical (NLO) applications due to their unique structural and electronic properties. These biomolecular materials possess strong hydrogen bonding, natural chirality and high transparency in the optical region. All these properties make them suitable for producing efficient second and third-order NLO responses [1-4]. Additionally, the zwitterionic nature of amino acids enhances molecular alignment and stability in the crystalline state, thereby improving phase-matching conditions for frequency-conversion processes [5]. Their biocompatibility, ease of crystallization and environmentally friendly properties further render them more suitable for the development of advanced photonic and optoelectronic devices [6]. Consequently, researchers are actively exploring amino acid-based NLO materials to achieve high-performance optical functionalities through sustainable and chemical approaches. In this context, special attention has been given to L-Serine, a naturally occurring amino acid, is frequently combined with picric acid to form organic salt crystals due to its zwitterionic nature and strong hydrogen bonding. The interaction between the proton-donating hydroxyl and amine groups of L-serine and the highly acidic picric acid promotes the formation of stable charge-transfer complexes, enhancing the structural integrity of the crystals. These organic salts exhibit improved physicochemical properties, including increased thermal stability, optical transparency and optimised NLO responses [7, 8]. Picric acid (2,4,6-Trinitrophenol, $C_6H_2(NO_2)_3OH$) is an organic compound made up of a benzene ring with three nitro ($-NO_2$) groups and a hydroxyl (-OH) group, classifying it as an aromatic organic molecule [9, 10]. The solution growth technique is widely used to form crystal salts for optical applications, owing to its ability to produce high-purity, defect-free crystals with excellent transparency. This method allows precise control over the crystallisation process by optimising parameters such as temperature, solvent selection and supersaturation levels, ensuring uniform growth with minimal internal stresses. Its cost-effectiveness, simplicity and scalability make it a preferred technique for developing high-quality materials for photonic and optoelectronic applications. In exploring nonlinear optical materials, various amino acids have been combined with picric acid to form organic salt crystals [11-15]. For example, L-arginine picrate has been examined for its promising nonlinear optical properties [16], while L-histidine picrate has been investigated for its structural and optical characteristics [17]. These studies

underscore the potential of amino acid-picric acid complexes in developing advanced materials for optical applications. Based on the literature survey, only the structural properties of the L-serinium picrate monohydrate (LSPM) crystal have been reported so far. Therefore, the present study focuses on investigating additional characteristics of LSPM, including UV–Vis–NIR optical absorption, lattice strain analysis, photoluminescence behaviour, thermal stability of the grown crystal and SHG efficiency.

2. Experimental details

2.1. Synthesis and Growth of LSPM single crystal

The slow evaporation technique is a preferred method for producing high-quality, well-ordered single crystals with a simple, low-cost setup. Analytical-grade L-serine and picric acid (99.9%) were used in the experimental setup. L-serine and picric acid with a molar ratio (1.3:1) were dissolved in double-distilled water at ambient temperature with continuous stirring using a magnetic stirrer equipped with a hot plate. The resulting solution was filtered to eliminate undissolved particles and allowed to settle at room temperature. The clear filtrate was transferred into a clean beaker and covered with Whatman filter paper to regulate the evaporation rate. The solution was kept undisturbed in a dust-free environment at room temperature. The slow solvent evaporation led to supersaturation, initiating growth. After 10 days, single crystals of L-serinium picrate monohydrate (LSPM) were obtained. The collected crystals were dried in a desiccator to remove residual moisture. The photograph of the grown crystals is shown in Fig. 1. The dimensions of the large crystal are approximately 18 × 9 × 3 mm³. The synthesis approach ensures the purity and stability of L-serinium picrate monohydrate crystals, making them suitable for the characterization studies. Reaction formula:

$$C_3H_7NO_3 + C_6H_2(NO_2)_3OH) \rightarrow C_3H_8NO_3 \cdot C_6H_2N_3O_7 \cdot H_2O \quad (1)$$

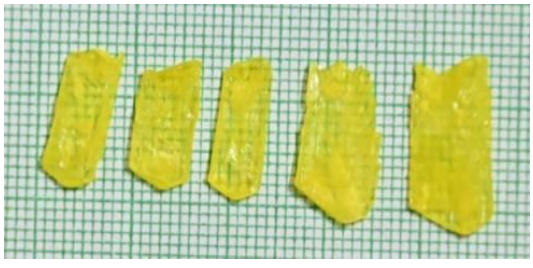

Fig. 1. Photograph of as-grown LSPM crystals (colour online)

2.2. Characterization techniques

The crystal structure was studied using a single-crystal X-ray diffractometer with monochromatic MoKα radiation (λ = 0.71073 Å) from a D8 X-ray source. The required data were gathered using an Apex II CCD detector. The crystalline nature of the grown crystal was established with a Bruker D8 Advance, Panalytical X Pert3 powder diffractometer. The functional groups and crystal structure were analyzed using FTIR spectra obtained using a JASCO FT/IR-6600 type A spectrometer (Origin: JASCO, Data Type: Infrared Spectrum). The optical transparency was evaluated using a JASCO V-670 UV-VIS-NIR Spectrophotometer with high-speed scanning. The HITACHI F-7000 Fluorescence Spectrophotometer was used to analyze the photoluminescence behaviour. Thermal characteristics were studied using a NETZSCH STA 449 F3 Jupiter in a nitrogen atmosphere. Finally, Kurtz and Perry's powder technique was used to evaluate the SHG efficiency of the grown crystal.

3. Results and discussion

3.1. Single crystal XRD study

The synthesized crystal LSPM was subjected to a single-crystal XRD to determine its crystalline structure. The single XRD study confirmed the monoclinic system of the compound with a $P2_1$ space group. The unit cell parameters were determined as follows: a = 14.205 Å, b = 6.871 Å, c = 14.584 Å with angles α = 90°, β = 110°, γ = 90°. These lattice parameter values are in good agreement with the recent literature [18]. The structure was refined by least-squares, and the final R-factor confirmed the reliability of the data. The non-centrosymmetric space group was determined from the XRD study to confirm second-harmonic generation in the grown material.

3.2. Powder XRD study

The structural characterization of the synthesized LSPM crystal was also carried out using powder X-ray diffraction (PXRD) analysis. The diffraction pattern was recorded over 10° to 70° in 2θ, with a step size of 10° and a scanning speed of 2° per minute. The observed diffraction peaks confirm the crystalline nature of the sample and material purity. The PXRD pattern displays well-defined peaks at specific 2θ values, indicating the long-range ordered arrangement within the crystal lattice. The powder XRD pattern of LSPM is shown in Fig. 2.

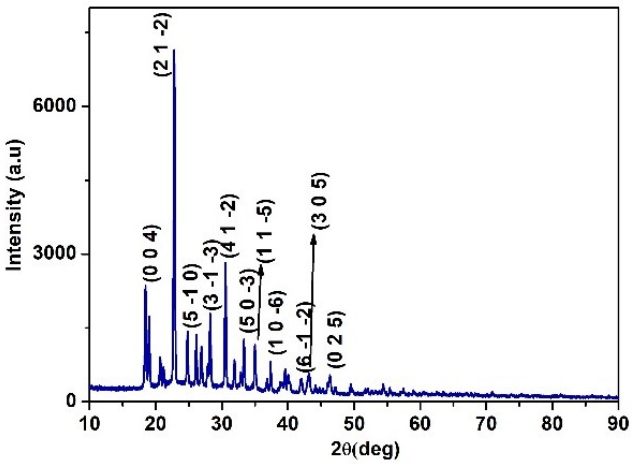

Fig. 2. Powder XRD pattern of LSPM (colour online)

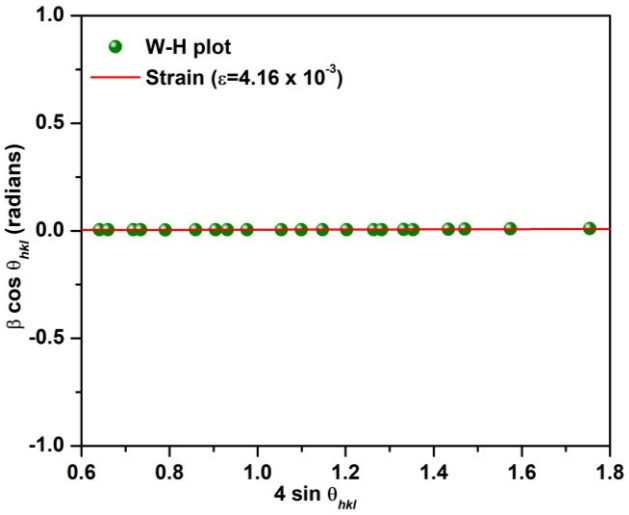

Fig. 3. W-H strain plot of LSPM (colour online)

The sharpness and intensity of the peaks ensure a higher degree of crystallinity. The diffraction peaks were indexed using standard crystallographic methods and the resulting d-spacing values were compared with reference data to validate the structural integrity of the material. The absence of additional peaks in the diffraction pattern indicates that the synthesized crystal is free from secondary phases or amorphous impurities, confirming the successful formation of the L-serinium picrate monohydrate crystal in its pure form [18]. The PXRD results provide reliable confirmation of the LSPM's crystalline phase and purity.

3.2.1. Williamson–Hall strain analysis of LSPM

To evaluate the contribution of crystallite size and lattice strain to the peak broadening observed in the PXRD pattern, the Williamson-Hall (W–H) method was employed [19]. The W-H equation is expressed as

$$\beta \cos\theta = \left(\frac{K\lambda}{D}\right) + 4\varepsilon \sin\theta \qquad (2)$$

where β is the full width at half maximum (FWHM) in radians, θ is the Bragg angle, K is the shape factor (0.9), λ is the X-ray wavelength, D is the crystallite size, and ε is the microstrain. A linear plot of $\beta \cos \theta$ versus $4 \sin \theta$ was constructed as shown in Fig. 3. The W-H strain plot of LSPM shows a slightly inclined horizontal line with negligible slope of the order 10^{-3}. Hence the plot ensures less lattice strain in the grown material. The magnitude of the strain (10^{-3} order) suggests moderate lattice distortion, which is commonly observed in organic molecular crystals due to intermolecular hydrogen bonding interactions. The relatively small strain value further confirms that the synthesized LSPM crystal possesses good crystalline quality, consistent with the sharp and well-defined diffraction peaks observed in the PXRD pattern.

3.3. FTIR study

Fourier Transform Infrared (FTIR) spectra of LSPM provide information to understand its molecular structure and presence of functional group. The FTIR spectra of LSPM are shown in Fig. 4. A broad absorption band observed at 3718, 3633, 3581 and 3454 cm^{-1} are attributed to O-H and N-H stretching vibrations, confirming the presence of hydrogen bonding within the crystal lattice. The peaks at 2991 cm^{-1} and 2895 cm^{-1} correspond to C-H stretching vibrations, indicating both aliphatic and aromatic hydrogen environments. The absorption bands at 1577 and 1410 cm^{-1} correspond to the asymmetric and symmetric stretching vibrations of carboxylate (COO^-) group, conforming deprotonating and salt formation. The band at 1460 cm^{-1} is attributed to $–CH_2$ bending vibrations, while the peak at 1331 cm^{-1} is assigned to C-N stretching, supporting the presence of amino functional groups in the crystal lattice. The absorption bands appearing at 1300 and 1331 cm^{-1} are assigned to C-N stretching vibrations, confirming the interaction between the amino acid and the picrate anion. The additional peaks below 1000 cm^{-1} correspond to out-of-plane bending vibrations of aromatic rings and C-H deformation modes. The FTIR spectral data confirm the formation of the L-serinium picrate structure, highlighting robust intermolecular interactions between the amino acid cation and the picrate anion, primarily through hydrogen bonding and electrostatic interactions [20-25]. Hydrogen bonding is an important factor for nonlinear optical properties because it helps align molecular dipoles in a crystal, leading to a non-centrosymmetric structure required for SHG. It can also enhance the electronic delocalization and charge transfer within molecules, further boosting NLO properties.

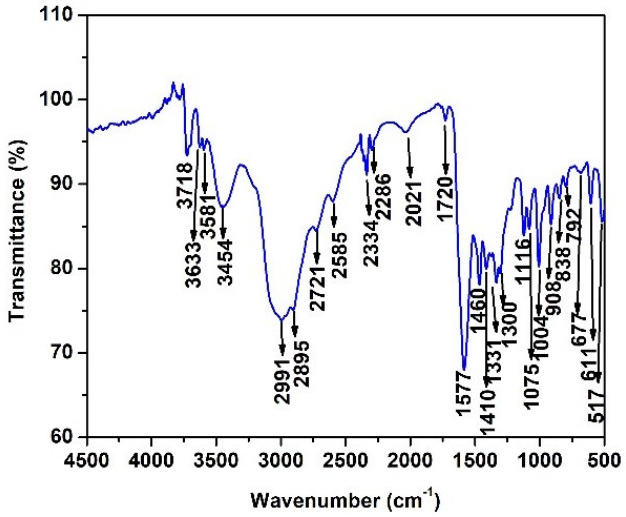

Fig. 4. FTIR spectra of LSPM (colour online)

3.4. UV-VIS-NIR spectral study

The UV-VIS-NIR spectra of L-serinium picrate monohydrate provide valuable information about its electronic transitions and optical properties. The absorption characteristics in the ultraviolet and visible regions provide critical information about the compounds electronic structure and interactions. The UV-VIS-NIR spectra of LSPM are shown in Fig. 5. The recorded spectrum shows significant absorption in UV region, followed by an extended dominant absorption edge into the visible region. In order to address the primary band edge transition, the absorption spectrum is plotted into Tauc plot using relation:

$$(\alpha h\nu)^2 = A(h\nu - E_g) \quad (3)$$

where α is the absorption coefficient, $h\nu$ is the photon energy, E_g is the optical band gap, A is a constant and n depends on the nature of electronic transition. To identify the transition type, the Tauc plot of $(\alpha h\nu)^n$ versus $h\nu$ was constructed, corresponding to a direct allowed transition ($n = 2$). The linear portion of the curve was extrapolated to intersect the energy axis $(\alpha h\nu)^2 = 0$. From this extrapolation, two absorption edge positions were observed 308 nm (4.025 eV) and 484 nm (2.56 eV). Among them, the 484 nm transitions is the primary transition, which is corresponds to the lowest-energy transition. Hence, it is considered as the fundamental optical band gap of the material, observed at 2.56 eV (E_g). Besides the fundamental transition, the secondary transition at 308 nm considered as higher energy transition with the excited state transitions. The recorded spectrum exhibits prominent absorption bands at 308 nm and 484 nm, which can be attributed to $\pi \rightarrow \pi^*$ and $n \rightarrow \pi^*$ electronic transitions associated with the molecular framework [26]. Thus, from the studies, the true optical band gap is associated with the long-wavelength absorption edge 484 nm [27, 28]. The obtained band gap value indicates that the material possesses a direct band gap in the visible region [29, 30]. The direct nature of the band gap implies efficient electronic transitions without phonon assistance, making the material potentially suitable for optoelectronic and photonic applications. Furthermore, the wide transparency window in the visible region supports its possible use in nonlinear optical and optical limiting devices. [31].

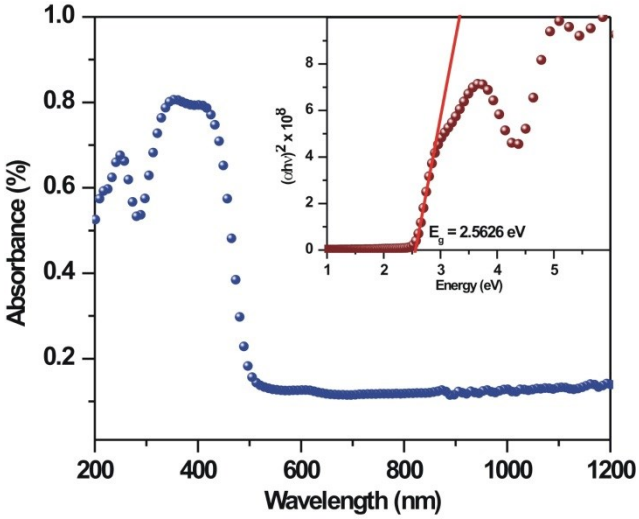

Fig. 5. The UV-VIS-NIR spectra of LSPM

3.5. Photoluminescence study

The photoluminescence study of LSPM was analyzed to determine its optical properties for prospective applications in optoelectronic and sensing technologies. Fig. 6 depicts the photoluminescence spectra of LSPM acquired at room temperature [32]. The excitation spectrum of LSPM exhibits a single prominent band centered at 402 nm, which is well fitted by a Gaussian function, indicating the presence of a dominant electronic excitation transition contributing to the observed fluorescence. The broad and single-band excitation with a Gaussian profile suggests that the multi-component emission leads to multiple relaxation pathways. As expected, the photoluminescence spectrum of LSPM recorded at room temperature reveals a structured multi-band emission extending from 470 to 610 nm, entirely within the blue-orange region of the visible spectrum. Spectral deconvolution resolved five distinct emissive components centered at 477, 498, 520, 560, and 603 nm and corresponding energy values are 2.6, 2.5, 2.4, 2.2 and 2.06 eV, respectively [33]. These values are slightly less than the value (2.56 eV) evaluated from Tauc plot. The broad blue-orange region of emission immediately

indicates that the fluorescence does not arise from simple localized π – π* transitions typical of isolated nitrobenzene derivatives, which generally emit in the UV or exhibit very weak visible fluorescence. The emission band centered at 477 nm appears in the blue region and exhibits a relatively narrow width (25 nm), suggesting a well-defined electronic transition with limited vibrational broadening. This band is attributed to higher-energy π–π* emission from the aromatic picrate system, likely corresponding to a localized singlet excited state ($S_1 \rightarrow S_o$). Owing to its higher energy and narrower profile, this transition may represent the least perturbed chromophoric emission in the system. The adjacent band at 497 nm shows a slight red shift relative to the 477 nm peak, along with increased intensity and a somewhat narrower width (20 nm). The small spectral separation between these two peaks supports the understanding of vibronic progression within the same excited state. Alternatively, this shift may reflect partial excited-state relaxation or stabilization through hydrogen-bond interactions within the crystal lattice. The emission is dominated by the intense band at 520 nm, which exhibits the largest integrated area and peak height. This feature is attributed to a stabilized charge-transfer excited state. The picrate anion contains strong electron-withdrawing nitro groups, while the L-serinium cation provides protonated amine functionality capable of electrostatic and hydrogen-bond interactions. Within the crystalline environment, these interactions promote intramolecular or intermolecular charge redistribution, leading to a stabilized charge-transfer state. The broad bandwidth of this emission further supports significant excited-state relaxation and structural reorganization prior to radiative decay. The lower-energy emissions at 560 and 603 nm are broader and weaker in intensity, suggesting further relaxation into deeper charge-transfer configurations or the presence of weak excimer or defect-related states in the solid phase. Their appearance indicates multiple emissive minima on the excited-state potential energy surface. Therefore, the progressive red shift from 477 to 603 nm, accompanied by spectral broadening, reflects substantial excited-state reorganization and strong environmental stabilization within the ionic crystal lattice. These findings confirm that LSPM exhibits multi-state fluorescence behavior governed by π–π* transitions, charge-transfer processes, and hydrogen-bond-mediated stabilization. The photo physical characteristics of LSPM therefore classify it as a solid-state, charge-transfer-active fluorophore with potential relevance for optical materials and fluorescence-based sensing applications.

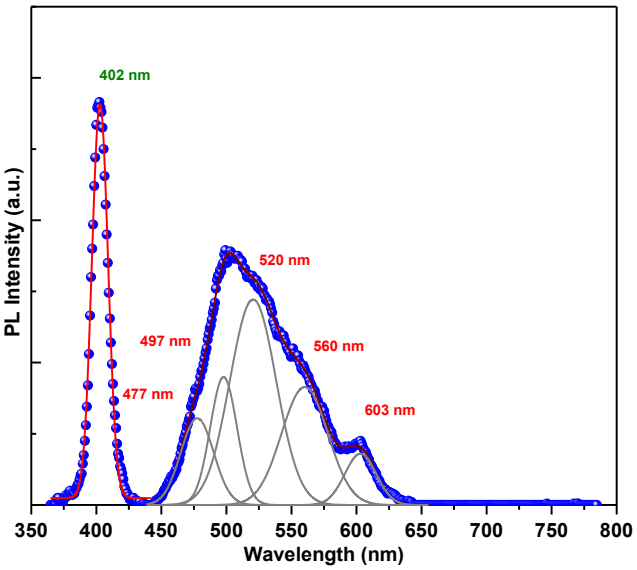

Fig. 6. Photoluminescence spectra of LSPM (colour online)

3.6. Thermal study

The thermal stability of the grown LSPM single crystal was examined using simultaneous thermogravimetric (TGA) and differential thermal (DTA) studies (Fig. 7) at temperatures ranging from 30 to 500 °C under nitrogen atmosphere.

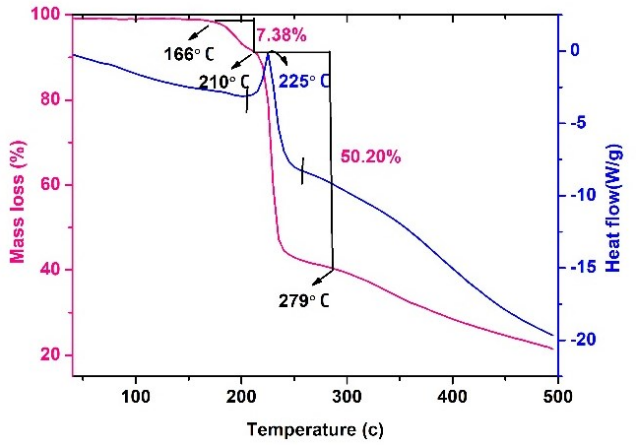

Fig. 7. TGA and DTA curves of LSPM (colour online)

The TGA curve demonstrates that the crystal decomposes in two steps. The initial weight loss of approximately 7.38% occurs between 166 °C and 210 °C, which can be attributed to the elimination of adsorbed or weakly bound water molecules, as well as potential lattice-entrapped solvents. The second substantial weight loss of about 50.2% occurs in the 220–280 °C regions, showing thermal degradation of the organic structure of the grown crystal LSPM. The DTA curve shows an endothermic peak at approximately 166 °C, which corresponds to the early dehydration phase. A fast endothermic event centred

at 225 °C, followed by a broad exothermic transition near 279 °C, is connected with picrate moiety breakage and subsequent material decomposition. Beyond 300 °C, the TGA curve shows a continuous mass loss, indicating further breakdown of the organic components, leading to a stable residual mass. The results show that the L-serinium picrate monohydrate crystal is thermally stable up to about 166 °C, after which it exhibits considerable structural disintegration. This stability range is sufficient for most nonlinear optical devices requiring moderate thermal endurance.

3.7. NLO study

The NLO efficiency of the grown crystal was measured using the popular Kurtz-Perry powder method [34]. In this method, the single crystal was crushed into fine powder to reduce orientation effects, ensuring that contributions from all crystallographic directions are efficiently collected during the second-harmonic generation (SHG). The powdered specimen was carefully packed into a capillary tube and exposed to the fundamental laser beam of a Q-switched Nd: YAG laser operating at 1064 nm. After irradiation, the material has shown nonlinear frequency doubling, emitting visible green light at 532 nm, corresponding to the second harmonic of the incident wavelength. The generated SHG signal was monitored with a photomultiplier tube, and an optical filter was used to remove any residual fundamental radiation, confirming the purity of the second-harmonic emission. For quantitative evaluation, the SHG of the sample was compared with that of a standard potassium dihydrogen phosphate (KDP) reference under identical experimental conditions. The measured efficiency of the grown crystal was approximately 1.5 times that of KDP. This NLO response demonstrates that the examined grown crystal has considerable nonlinear susceptibility and non-centrosymmetric ordering. Furthermore, compared with other published organic NLO crystals, the current material exhibits higher SHG efficiency, indicating that it combines the benefits of organic molecular flexibility with enhanced nonlinear response. These qualities make the compound a preferable choice for photonic and optoelectronic applications such as frequency conversion, optical switching and laser technology.

4. Conclusion

The structural, optical, thermal and nonlinear optical properties of L-serinium picrate monohydrate single crystals were thoroughly investigated. Single- crystal and powder XRD studies confirmed the non-centrosymmetric monoclinic structure and the W-H strain analysis ensure less lattice strain in the grown crystal. The FTIR study demonstrated the presence of functional groups which also ensured molecular dipole alignment and the formation of a charge-transfer complex through distinctive vibrational modes associated with hydrogen bonding. Optical and fluorescent investigations demonstrated high transparency, a reasonable band gap and stable emission properties. Thermal investigations have demonstrated compound's stability up to 166 °C enabling optoelectronic devices to be operated without damage. Kurtz-Perry powder technique measured the SHG efficiency as 1.5 times that of KDP, confirming the high nonlinear optical property of the material. Overall, these findings support LSPM as a better choice for photonic and optoelectronic applications due to its greater stability.

References

[1] M. Fleck, A. M. Petrosyan, "Salts of amino acids, Crystallization, Structure and Properties", Cham, Switzerland: Springer International Publishing **10**, 978 (2014).
[2] M. Takehara, Colloids and Surfaces **38**(1), 149 (1989).
[3] D. B. Tripathy, A. Mishra, J. Clark, T. Farmer, Comptes Rendus Chimie **21**(2), 112 (2018).
[4] G. S. Tonoyan, G. Giester, A. M. Petrosyan, Journal of Physics: Conference Series **2924**, 012007 (2024).
[5] H. M. Albert, C. A. Gonsago, Journal of Electronic Materials **51**(8), 4555 (2022).
[6] A. Islam, Z. Haider, M. Imran, M. D. Li, R. U. Hassan, Advanced Optical Materials **13**(3), 2401920 (2025).
[7] N. Tyagi, H. Yadav, A. Hussain, B. Kumar, Journal of Molecular Structure **1224**, 129190 (2021).
[8] H. M. Albert, S. Saarwin, C. A. Gonsago, Journal of Materials Science: Materials in Electronics **34**(18), 1407 (2023).
[9] A. Rakini, K. Rajarajan, M. Neela, B. Premalatha, S. Surya, Journal of Materials Science: Materials in Electronics, **35**(10), 706 (2024).
[10] A. Alexandar, I. Johnson, A. M. Dayana, T. S. Girisun, B. S. I. Lasalle, M. S. Pandian, Inorganic Chemistry Communications **159**, 111751 (2024).
[11] T. U. Devi, N. Lawrence, R. R. Babu, K. Ramamurthi, Journal of Crystal Growth **310** (1), 116 (2008).
[12] T. U. Devi, N. Lawrence, R. R. Babu, K. Ramamurthi, Spectrochimica Acta Part A: Molecular and Biomolecular Spectroscopy **71**(2), 340 (2008).
[13] G. Bhagavannarayana, B. Riscob, M. Shakir, Materials Chemistry and Physics **126**(1-2), 20 (2011).
[14] M. Silviya, S. Aswathappa, L. Sweatha, M. Anithalakshmi, V. Mowlika, R. Robert, Journal of Molecular Structure **1327**, 141168 (2025).
[15] A. M. Petrosyan, V. V. Ghazaryan, B. R. Srinivasan, Inorganic Chemistry Communications **166**, 112631 (2024).
[16] T. Martins, A. Araújo, S. Da Silva, J. D. R. Matos, P. C. Isolani, G. Vicentini, Journal of Solid State Chemistry **171**(1-2), 212 (2003).
[17] R. Subaranjani, J. Madhavan, S. Prathap, M. V. A. Raj, Materials Today: Proceedings **8**, 456 (2019).

[18] B. Zakharov, V. Ghazaryan, E. Boldyreva, A. Petrosyan, Journal of Molecular Structure **1100**, 255 (2015).
[19] N. Sivakumar, Dinesh Kumar, Rajesh Maurya, Subhashis Saha, Trilok Singh, Jatindra Kumar Rath, Journal of Materials Science: Materials in Electronics **36**, 973 (2025).
[20] A. Hemalatha, S. Arulmani, K. Deepa, D. S. Kumar, J. Madavan, S. Senthil, Materials Today: Proceedings **8**, 142 (2019).
[21] N. Kanagathara, M. Marchewka, J. Janczak, K. Senthilkumar, Physica B: Condensed Matter **679**, 415807 (2024).
[22] B. Ravindran, R. A. Shiny, T. B. Beno, N. Lavanya, Materials Today: Proceedings **80**, 3634 (2023).
[23] N. Sivakumar, J. Srividya, J. Mohana, G. Anbalagan, Spectrochimica Acta Part A: Molecular and Biomolecular Spectroscopy **139**, 156 (2015).
[24] Jagadesan, N. Sivakumar, S. Arjunan, G. Parthipan, Optical Materials **109**, 110285 (2020).
[25] N. Sivakumar, J. Venkatamuthukumar, Magesh Murugesan, Ali Alsalme, Optical Materials **122**, 111730 (2021).
[26] A. Jezuita, H. Szatylowicz, T. M. Krygowski, Chemical Physics Letters **753**, 137567 (2020).
[27] P. Krishnan, K. Gayathri, N. Sivakumar, S. Gunasekaran, G. Anbalagan, Journal of Crystal Growth **396**, 85 (2014).
[28] N. Sivakumar, V. Jayaramakrishnan, K. Baskar, G. Anbalagan, Optical Materials **37**, 780 (2014).
[29] H.-P. Hsu, L.-C. Li, M. Shellaiah, K. W. Sun, Scientific Reports **9**, 13311 (2019).
[30] B. D. Viezbicke, S. Patel, B. E. Davis, D. P. Birnie III, Physica Status Solidi (B) **252**, 1700 (2015).
[31] Y. G. Sıdır, İ. Sıdır, Journal of Fluorescence **35**, 8269 (2025).
[32] N. Sivakumar, G. Anbalagan, Optical Materials **60**, 533 (2016).
[33] A. Jagadesan, N. Sivakumar, R. M. Kumar, G. Chakkaravarthi, S. Arjunan, Optical Materials **84**, 864 (2018).
[34] S. Kurtz, T. Perry, Journal of Applied Physics **39**, 3798 (1968).

*Corresponding author: vasudevan.p@rajalakshmi.edu.in
vasuskr@gmail.com